

On the Dispersal of Young Stellar Hierarchies

Bruce G. Elmegreen

*IBM T. J. Watson Research Center, 1101 Kitchawan Road, Yorktown Heights, New York
10598 USA*

`bge@us.ibm.com`

ABSTRACT

Hierarchical structure in young star fields has been demonstrated in a variety of ways, including two point correlation functions (TPCFs) that are power laws for spatial scales up to at least several hundred parsecs. As the stars age, this power law decreases in slope until it becomes nearly flat at ~ 100 Myr, at which point the hierarchical structure has disappeared. The fact that the TPCF remains nearly a power law during this time implies that the dispersal mechanism is somewhat independent of scale. This rules out dispersal by random stellar motions at either the local gas turbulent speed or a constant speed, because in both cases the hierarchy would disappear at small scales first, causing the TPCF to bend over. Destruction by shear has the right property as the shear rate in a galaxy is independent of scale for kpc-size regions, but shear converts the hierarchy into an azimuthal stream which still has a power-law TPCF. What does explain the observation is the overlapping of several independent hierarchies from successive generations of star formation in the same region. If stellar age is determined from magnitude intervals on the main sequence of a color-magnitude diagram, or if clusters ages are grouped together logarithmically into bins, then multiple generations will overlap more and more as the grouped populations age, and this overlap will lower the spatial correlations between group members. Models of these processes illustrate their relative roles in removing the appearance of young stellar hierarchies.

Subject headings: stars: formation — open clusters and associations: general — galaxies: star clusters: general — galaxies: star formation

1. Introduction

Young stars tend to be grouped together into a hierarchy of scales where smaller and denser sub-regions are inside larger and looser regions, spanning a wide range from star

clusters and their initial subclumps at ~ 1 parsec scales and smaller, to OB associations at ~ 10 parsecs, to star complexes at ~ 100 parsecs, to flocculent spiral arms on the largest scale (see review in Elmegreen 2010).

Hierarchical structure on large scales was observed for whole OB associations in the LMC (Feitzinger & Braunsfurth 1984), HII regions in 19 galaxies (Feitzinger & Galinski 1987) and 93 galaxies (Sánchez & Alfaro 2008), stellar groupings determined from near-neighbor path linkage in M31 (Battinelli et al. 1996), NGC 300 (Pietrzyn’ski et al. 2001), and in seven other galaxies (Bresolin et al. 1998), and star complexes using flux contours in M51 (Bastian et al. 2005) and in nine other galaxies (Gusev 2002). It was also observed using stellar density contours in the LMC (Maragoudaki et al. 1998) and M33 (Ivanov 2005), and box counting techniques in 10 galaxies (Elmegreen & Elmegreen 2001), 14 galaxies (Elmegreen et al. 2014) and at high resolution in NGC 628 (Elmegreen et al. 2006). It was observed with Fourier transform power spectra of optical light in six galaxies (Elmegreen et al. 2003a), optical and H α light in nine dwarf irregulars (Willett et al. 2005), and optical light at high resolution in M33 (Elmegreen et al. 2003b). These studies looked primarily at the positions of star-forming regions and did not consider the time evolution of this structure.

Hierarchical structure among individual stars gives some information about evolution because a star’s position on the main sequence of a color-magnitude diagram gives an upper limit to its age. Stellar hierarchies have been observed in M33 and NGC 6822 using minimum spanning trees (Bastian et al. 2007; Gouliermis, et al. 2010), in the LMC (Harris & Zaritsky 1999; Bastian et al. 2009) and SMC (Gieles et al. 2008) using several methods including the Q parameter from Cartwright & Whitworth (2004) and the two point correlation function (TPCF), in NGC 6503 and NGC 1566 with the TPCF (Gouliermis et al. 2015, 2017), in four (Odekon 2006) and six (Bastian et al. 2011) dwarf irregular galaxies using the TPCF or Q parameter, and in the LMC, SMC, M31 and M33 over at least two orders of magnitude in scale with the TPCF (Odelon 2008).

Individual star forming regions in the SMC (Gouliermis et al. 2012) and Milky Way (Gomez et al. 1983; Larson 1995; Simon 1997; Gomez & Lada 1998; Bate et al. 1998; Johnstone 2000; Testi et al. 2000; Smith et al. 2005) were also shown to be hierarchical on smaller scales using the TPCF. Sub-structure has been noted in resolved OB associations and clusters too (e.g., Heydari-Malayeri 2001; Nanda Kumar et al. 2004; Dahm & Simon 2005; Gutermuth et al. 2008). Embedded stars tend to follow the fractal structure of the clouds in which they form (Sánchez, et al. 2007; Fernandes et al. 2012; Gregorio-Hetem et al. 2015). Stellar multiplicity (e.g., Brandeker et al. 2003) could be the small scale limit of hierarchical structure.

Generally, these studies find that hierarchical structure in stars disappears gradually

over time, taking around 100 Myr for scales between ~ 1 pc and several hundred parsecs. Substructure in open clusters disappears over time too (Sánchez & Alfaro 2009, 2010). Observations of clustering in red supergiants and Cepheid variables (Payne-Gaposchkin 1974; Efremov 1978; Elmegreen & Efremov 1996), for which individual ages may be derived, were reviewed by Efremov (1995); usually there are not enough of these stars in any one region to see levels of substructure.

Position and time correlations among clusters give the most detailed picture of evolution because each cluster has an age. Zhang et al. (2001) used the TPCF to show hierarchical structure up to ~ 0.7 kpc and 160 Myr for clusters in the Antennae galaxy; there was no clear variation with age in that range although massive young stars less than 10 Myr old had less correlation than the clusters. Scheepmaker et al. (2009) measured the TPCF in M51 for clusters in three logarithmic age bins up to 400 Myr and found that older clusters were slightly less correlated than younger clusters on scales larger than 160 pc. Grasha et al. (2015) showed a strong two-point correlation from the limit of resolution at 0.2 arcsec (9.6 pc) up to 100 arcsec (4800 pc) for Class 3 clusters (which are young and possibly unbound) in NGC 628. Grasha et al. (2017a) found similar correlations for all resolved separations below ~ 1 kpc for young stellar groupings in 5 other galaxies, and showed that this upper limit increases with galaxy size, ranging from several hundred parsecs in NGC 7793 and NGC 3738 to several thousand parsecs in NGC 1566 and NGC 628.

The decrease in spatial correlation between clusters with increasing age suggests not only that older clusters are more randomly positioned than younger clusters, but also that clusters close to each other in space tend to be younger, which means that they have more similar ages than clusters that are far from each other. This correlation is such that the age difference, ΔT , between sub-regions in a hierarchy of star formation increases approximately as their spatial separation, ΔS , to some power. In the LMC, $\Delta T = 2.9\Delta S^{0.33}$ between $\Delta T \sim 8$ Myr at $\Delta S \sim 20$ pc and $\Delta T \sim 30$ Myr at $\Delta S \sim 1$ kpc (Efremov & Elmegreen 1998). In the local Milky Way, $\Delta T = 10.6\Delta S^{0.16}$ from ~ 20 Myr at ~ 50 pc to ~ 30 Myr at ~ 600 pc (de la Fuente Marcos & de la Fuente Marcos 2009). In 8 other galaxies, $\Delta T \sim 5.0\Delta S^{0.38}$ from an average age difference of ~ 8.6 Myr at ~ 4.2 pc to ~ 55 Myr at ~ 550 pc (Grasha et al. 2017b). These power laws are reminiscent of the correlation between the crossing time inside a molecular cloud, T_{cross} , and the cloud radius, R . The crossing time is the ratio of twice the cloud radius, $2R$, to the internal velocity dispersion, σ . For the Milky Way, $\sigma = 0.48(R/\text{pc})^{0.63\pm 0.30}$ km s $^{-1}$ for $R = 1$ to 200 pc (Miville-Deschênes et al. 2017), so $T_{\text{cross}} = 4.1R^{0.37}$ Myr for molecular clouds. This implies $\Delta T \sim T_{\text{cross}}$ for young regions (see also Elmegreen 2000).

All of these correlations for young stars and clusters disappear as the stars and clusters

age. This seems at first a reasonable expectation because of random motions. However, random motions produce an expectation that is not observed, namely that smaller scales should lose their correlated structures before larger scales. This is because in a given scale, λ , random mixing removes substructures smaller than the mixing time, $\tau = \lambda/\sigma$, for velocity dispersion σ , and it does not significantly remove structures larger than this. Thus the power law TPCF should have a break and turn over on scales smaller than $\tau\sigma$, and this turn-over distance should increase linearly with time if σ is independent of scale, and as the second power of time if $\sigma \propto \lambda^{0.5}$. Observations of the time dependence of stellar correlations (Gieles et al. 2008; Gouliermis et al. 2015, 2017) show that the TPCF remains a power law, however. The TPCF amplitude decreases uniformly over time while preserving the power law (see also Bastian et al. 2009, 2011), which implies that every scale gets washed out simultaneously.

Another process that can remove correlated structure is shear. Indeed, Grasha et al. (2017b) found that the ratio of the maximum spatial separation in the time-space correlation for young clusters to the cluster age difference is always about equal to the relative velocity from shear on this maximum scale. That is, the maximum age difference for the observed correlation is always about the inverse of the Oort A shear parameter for the 8 galaxies they studied. Shear has the attractive property that the shear rate is independent of scale, since A does not vary much on scales below a kiloparsec or so. Thus shear could decrease the amplitude of the TPCF uniformly with time, preserving the power law. However, shear just stretches the initial structure in the azimuthal direction, removing the radial component of the correlation and not the azimuthal component, so the decrease in TPCF cannot go to zero amplitude, only to the correlation amplitude expected for a 1-dimensional fractal. Shear plus random motion also has the wrong property because the time-dependent turn-over at small scales would still be present from the random motions.

A third possibility is that the correlated structure in aging star fields disappears because new regions of star formation with new correlations occur on top of the old regions. This *superposition* removes the correlation of the summed distribution in a scale-independent way over time, decreasing the amplitude of the total TPCF to zero if the overlap is large enough. Selecting stellar age groups from the color-magnitude diagram, which has been the usual procedure for some of the above papers, can have this superposition effect because low mass stars can be both old according to their main-sequence turn off positions, and young as members of more recently formed groups (e.g., Bastian et al. 2011). Selecting stellar ages in logarithmic intervals also has this effect because the time interval for the selection increases with age, and so the number of separate star-forming episodes in each region increases with age too. TPCFs for clusters can in principle get around this blending effect because the ages are known and different age groups can be examined separately. However, the number of

clusters at small separations is usually low at the older ages, so any predicted small-scale turnover in the TPCF, e.g., from random motions, might be difficult to see.

In what follows, Section 2.1 discusses the model, Sections 2.2 and 2.3 show the effects of random stellar motions and shear, and Section 2.4 models the superposition of stellar populations, without and with the inclusion of random motions and shear. The conclusions are in Section 3.

2. A Model for Hierarchical Distributions

2.1. Setup

The effects of random motion, shear, and superposition on the TPCF are studied here in the shearing sheet approximation for a piece of a galaxy. The initial distribution of young stars is taken to be a random fractal on a plane made by selecting, in a hierarchy of steps, N_f subcells inside each cell with a decrease in cell size equal to a factor of $f = 1/2$ at each step. The fractal dimension in this case is $-\log N_f / \log f$.

In a typical model, the sheet consists of 512 by 512 lowest-level cells with 8 ($1 + \log_2 512/4$) sub-levels of hierarchy. The highest level has 16 cells, i.e., 4×4 with side lengths of 128 cell-lengths each, and these 16 cells are independent. Lower levels have $2^i \times 2^i$ cells of $512/2^i$ cell-lengths each, for $i = 3$ to 9. Starting with the 4×4 cells, a number of them is chosen to contain young stars in their sublevels. This number has an average value of $p \times 4 \times 4$ where $p = 2^{D_f-2}$ is the probability of choice determined by the fractal dimension D_f . For example, if the fractal dimension is $D_f = 2$, then $p = 1$ and all cells are chosen, filling in the grid completely. We pick $D_f = 1.3$ here in analogy with interstellar clouds (Elmegreen & Falgarone 1996), and then $p = 0.62$. The cells are chosen by cycling through each one and picking a random number uniformly distributed between 0 and 1, and then determining if that random number is larger or smaller than p . If it is smaller, than we use that cell for subsequent division into subcells, and if it is larger, we ignore that cell during further steps. We next cycle through each of the chosen cells from this 4×4 level to pick subcells in the next lower level. Again we pick a random number for each possible subcell and compare it to p . After we have this next list of chosen cells, we cycle through each of those, picking sub-subcells with the same probability p . Eventually we get to the lowest cell in the grid, which cannot be subdivided. We consider each of the chosen lowest-level cells to contain one object whose TPCF is to be measured, i.e., a star or a cluster. For convenience, the size of the overall grid is normalized to 1, which means that each cell has a size of $1/2^i$ for $i = 2$ on the largest scale to $i = 9$ on the smallest scale.

Once the cells with stars are chosen, the TPCF is determined by cycling through each star (called the “first star” here) and counting the number of other stars (the “second star”) within certain intervals of distance. These intervals are equally spaced in units of the log of the distance. To avoid boundary effects, we pick only first stars between the limits of 0.25 and 0.75 times the grid coordinates, and consider distances between these first stars and the second stars only up to 0.25 of the grid size. Thus the range of possible distances between stars is 0.25 of the grid size, or 128 cell units. This is the maximum spatial range of the power law in the resulting TPCF. For a uniform distribution of stars in the plane, the number of pairs increases with distance to the power 2 for logarithmic distance intervals. To find the excess correlation above this uniform value, we make a histogram of log-distances by summing $(0.25/D)^2$ for each pair with distance D (recall that the longest distance is 0.25). We confirmed that for a uniform distribution of stars, the histogram is flat. This procedure gives the initial TPCF, i.e., at the beginning of the time evolution before random motions, shear, or superposition are included.

2.2. Random Motions

To simulate the effects of stellar motions with a random turbulent velocity, the stars in each hierarchical level i from 2 to 9 were moved for a distance given by a simulated velocity dispersion, σ_i , that depends on the level. Recall that the cells have sizes $1/2^i$, so we choose σ_i to scale with the square root of the cell size. Thus all of the stars in each cell of level i move because of initial cloud turbulence at that level, and they move for a distance in the x direction equal to $\sigma_0/2^{i/2}$ times a random variable between -0.5 and 0.5 . Similarly, they move for a distance in the y direction equal to this same fiducial value times another random variable between -0.5 and 0.5 . This motion occurs hierarchically, which means that all of the stars in each large cell, with $i = 2$, move together, although each large cell moves differently. At the same time, all of these stars move again for a shorter distance in batches according to their groupings in the next-smaller cells, which have $i = 3$. The same stars move again with smaller distances grouped into the $i = 4$ cell, and so on until the $i = 9$ cell, which contains only one star. These single stars finally move once again over the smallest relative distance. Thus each star has 8 contributions to its total motion, each in a random direction, and one for each of the 8 cells it is in with one cell per hierarchical level from $i = 2$ to 9. These 8 contributions reflect the concept that turbulence consists of smaller scale motions inside larger scale motions, and that stars are born with a motion equal to that of the cloud in which they form.

Figure 1 shows the TPCF and its evolution with random motions. The initial distribu-

tion for one of ten trial fractals is shown by the red points in each panel. The initial TPCF is shown by a red histogram in the lower right; this is the average of 10 histograms made from different random initial conditions. The TPCF is a power law with a slope $\gamma = -0.7$, as expected for the initial fractal distribution, which has a fractal dimension of $D_f = 1.3$ ($\gamma = D_f - 2$ in two dimensions). The distribution after random motions with amplitude $\sigma_0 = 4$ is shown by the blue points in the upper right and the blue histogram (also an average of 10 histograms). The distribution with $\sigma_0 = 10$ is shown by the green points in the lower left and the green average histogram. The main effect of random motions on the TPCF is a turnover at small scale, with increasing scale for the turnover at larger random motions. Larger random excursions in our model correspond to older stars, as they have moved further from their origins (ignoring epicycles).

2.3. Shear

To simulate the effects of shear, we move each star for a distance in the x direction (horizontal in the figures, and azimuthal in the galaxy) given by $\Delta x = A(y - 0.5)$ (where y is vertical in the figures and radial in the galaxy). This motion is independent of the level of the hierarchy and it assumes that each star forms at the same time.

Figure 2 shows the result. The red points in the left and middle panels and the red histogram are the same initial positions and TPCF as in Figure 1. The blue points on the left correspond to $A = 1$ and are compared to the red points in the same panel. The green points in the middle panel are for $A = 5$. Blue and green histograms show the corresponding TPCFs. The TPCFs are averages of 10 trials with random initial conditions. Note that $A = 1$ corresponds to a horizontal motion of 0.5 times the total grid size in the rightward direction at the top of the grid and the same motion to the left at the bottom of the grid. The transformation of red points to blue points on the left shows the patches moving toward a 45 degree angle. Points that move off the grid to the left and right are wrapped around to the other side. For the larger shear value, $A = 5$ in the middle panel, points near the top and bottom of the grid have been wrapped around many times.

The histograms decrease in amplitude with increasing shear, but they do not change significantly in slope and the changes are not very fast. This is because local regions do not shear much within themselves but tend to lose correlation first with the more distant regions. Thus the power law flattens most on large scales and it does not change much on small scales. Also, stars that are initially correlated in the azimuthal direction do not lose their correlation because their relative positions do not change with shear.

2.4. Superposition

After stars form in a region, the gas that formed them moves around and later forms new stars. Presumably this is a continuous process for a steady star formation rate, and presumably each new generation is somewhat independent of the old one. Here we determine the TPCF for stars made in several generations. We first show the result without random motions or shear, and then we add these additional effects.

Figure 3 shows the result of superposition alone for 20 generations. The top left shows the positions of stars in the 20th (last to form) and 19th (second last to form) generations as red and blue points. Without random motion or shear, they have not moved. The red histogram in the lower right shows the TPCF for this 20th generation; it is a power law because the stars have their original fractal distribution. The blue histogram in the lower right is the TPCF for the sum of the two generations, i.e., the red and blue points together. The TPCF is still the same power law on small and intermediate scales because each generation still has structure on these scales and there is little overlap between the two. The TPCF for the superposition decreases on large scales, however, because there is no correlation between stars in the 20th generation and stars in the 19th generation, and these intergenerational spacings tend to have large scales when only two generations are involved.

The top right of Figure 3 shows star positions for the 1st (first to form) and 11th generations in magenta and green, respectively. These distribution also appear with their original fractal forms because there is no random motion and shear. The green and magenta histograms in the lower right are from a superposition of the first 11 generations and all 20 generations, respectively. With more generations added, the large-scale flattening of the TPCF spreads to smaller scales as the uncorrelated overlapping regions become more dense. The lower left panel shows all 20 generations superposed; this is what made the magenta histogram.

The effects of superposition with random motions are shown in Figure 4. The random distance increases with time, so in a stack of 20 generations the oldest stars ($j = 1$ generation) have moved the most and the youngest ($j = 20$ generation) not at all. A motion rate corresponding to $\sigma_0 = 10$ after 20 generations is used (i.e., $\sigma_0 = (N - j)/2$ for the j -th generation out of $N = 20$). The colors in Figure 4 represent the same generations as in Figure 3. In the top left, the most recent generations to form (20th and 19th) have little or no random motions, and their histograms (red and blue) are nearly power laws. In the top right panel, the 1st generation (magenta) is very dispersed and the 11th generation (green) less so. Their TPCFs are in the lower right with the same colors.

Figure 5 shows superposition and random motions as in Figure 4, but now also with

shear given by $A = (N - j)/20$, which is about the same amount of shear for the oldest stars ($j = 1$) as in the left panel of Figure 2, where $A = 1$. The effects of shear can be seen in the stellar distributions, especially for the magenta points ($j = 1$) in the upper right panel, but it does not change the TPCF much compared to the case of superposition plus random motion without shear.

3. Conclusions

Several processes in galaxy disks cause young stars and clusters to decrease their two point correlation over time. Random stellar motions acquired at birth can do this, producing a bend in the TPCF at small scales where the random motions are relatively fast for their length scale. Because observations by Bastian et al. (2011), Gouliermis et al. (2015), Gouliermis et al. (2017) and others do not show such a bend, random motion alone is probably not the only process at work. The TPCF for clusters in Grasha et al. (2015, 2017a) also shows no bend at small scales, although the uncertainty is large because the number of clusters is small.

Shear would seem to remove correlations in the positions of young stars, and Grasha et al. (2017b) show that the average shear velocity in a region corresponds to the ratio of the maximum correlated length to the maximum cluster age difference at that length. However shear in our models does not appear to affect the TPCF very much. Shear causes the more distant stars and clusters to move for a larger relative distance than the nearby stars and clusters, so it flattens the TPCF on large scales first. However, it takes a lot of shear to change the TPCF noticeably, and the correlations in the azimuthal direction are not changed at all.

Superposition of multiple generations seems to affect the TPCF most, especially when combined with random motion (Fig. 4). Shear can be present also, but it does not contribute much more (Fig. 5). This result applies when stars with a wide range of ages are included in the TPCF, because then the younger stars are likely to have formed in a different hierarchy of interstellar gas than the older stars. Continuous star formation should have this property, so the appearance of a power law TPCF with a shallow slope may indicate that the objects included in that TPCF have been forming continuously for the duration of the sample. Star formation that occurred in the recent past with no younger stars superposed should have a power-law TPCF with a bend at small scales from random stellar motion. Thus, there should be a relationship between the history of star formation and the shape of the TPCF when the crossing time for random stellar motions increases with scale.

An exception to this result occurs if the stars are in a gravitationally bound cluster with

a radial density profile. Then the TPCF can remain a power law on small scales even though the stars are mixed and have lost their initial hierarchy. The TPCF bends over only when random stellar motions move stars away from each other.

In summary, the model predicts that a bend should appear on small scales in the TPCF for young objects that are in a small age interval so that they formed nearly simultaneously. The bend is from random stellar motions or random cluster motions in an initially turbulent interstellar gas. The bend may not appear for objects in a large age interval, which includes stars chosen from their appearance on the main sequence of a color-magnitude diagram. Stellar magnitude gives only an upper limit to the stellar age, which is the turn-off age for that star, so a range of ages is possible among main sequence stars with the same magnitude. When there is a range of ages like this, then the superposition of a power-law TPCF from each age interval will diminish the correlation and flatten the function for the whole sample, starting with the largest scales first and then moving toward smaller scales as more independent star formation epochs are added together and the overlap becomes denser.

REFERENCES

- Bastian, N., Gieles, M., Efremov, Yu. N., & Lamers, H. J. G. L. M. 2005, *A&A*, 443, 79
- Bastian, N., Ercolano, B., Gieles, M., Rosolowsky, E., Scheepmaker, R. A., Gutermuth, R., & Efremov, Yu. 2007, *MNRAS*, 379, 1302
- Bastian, N., Gieles, M., Ercolano, B., & Gutermuth, R. 2009, *MNRAS*, 392, 868
- Bastian, N., Weisz, D. R., Skillman, E. D., McQuinn, K. B. W., Dolphin, A. E., Gutermuth, R. A., Cannon, J. M., Ercolano, B., Gieles, M., Kennicutt, R. C., & Walter, F. 2011, *MNRAS*, 412, 1539
- Bate, M. R., Clarke, C. J., & McCaughrean, M. J. 1998, *MNRAS*, 297, 1163
- Battinelli, P., Efremov, Y., & Magnier, E.A. 1996, *A&A*, 314, 51
- Brandeker, A., Jayawardhana, R., & Najita, J. 2003, *AJ*, 126, 2009
- Bresolin, F., Kennicutt, R.C., Jr., Ferrarese, L., Gibson, B. K., Graham, J. A., Macri, L. M., Phelps, R. L., Rawson, D. M., Sakai, S., Silbermann, N. A., and 2 coauthors 1998, *AJ*, 116, 119
- Cartwright A., & Whitworth A. P., 2004, *MNRAS*, 348, 589

- Dahm, S.E., & Simon, T. 2005, AJ, 129, 829
- de la Fuente Marcos, R., & de la Fuente Marcos, C. 2009, ApJ, 700, 436
- Efremov, Y.N. 1978, Sov. Astron. Lett., 4, 66
- Efremov, Y.N., 1995, AJ, 110, 2757
- Efremov, Y. N., & Elmegreen, B. G. 1998, MNRAS, 299, 588
- Elmegreen, B.G. & Efremov, Yu.N. 1996, ApJ, 466, 802
- Elmegreen, B.G. & Falgarone, E. 1996, ApJ, 471, 816
- Elmegreen, B.G. 2000, ApJ, 530, 277
- Elmegreen, B.G. & Elmegreen, D. M. 2001, AJ, 121, 1507
- Elmegreen, B. G., Elmegreen, D. M., & Leitner, S. 2003a, ApJ, 590, 271
- Elmegreen, B.G., Leitner, S.N., Elmegreen, D.M. & Cuillandre, J.-C. 2003b, ApJ, 593, 333
- Elmegreen, B.G., Elmegreen, D.M., Chandar, R., Whitmore, B., & Regan, M. 2006, ApJ, 644, 879
- Elmegreen, B.G. 2010, in IAUS266, Star Clusters Basic Galactic Building Blocks Throughout Time And Space, eds. Richard de Grijs and Jacques Lepine, Cambridge University Press, pp 3-13
- Elmegreen, D. M., Elmegreen, B. G., Adamo, A., et al. 2014, ApJL, 787, L15
- Feitzinger, J. V., & Braunsfurth, E. 1984, A&A, 139, 104
- Feitzinger, J. V. & Galinski, T. 1987, A&A, 179, 249
- Fernandes, B., Gregorio-Hetem, J., Hetem, A. 2012, A&A, 541A, 95
- Gieles M., Bastian N., & Ercolano E. 2008, MNRAS, 391, L93
- Gomez, M., Hartmann, L., Kenyon, S. J. & Hewett, R. 1993, AJ, 105, 1927
- Gomez, M. & Lada, C.J. 1998, AJ, 155, 1524
- Gouliermis, D.A., Schmeja, S., Klessen, R.S., de Blok, W.J.G., Walter, F. 2010, ApJ, 725, 1717

- Gouliermis, D.A., Schmeja, S., Dolphin, A.E., Gennaro, M., Tognelli, E., Prada Moroni, P.G. 2012, *ApJ*, 748, 64
- Gouliermis, D.A., David Thilker, D., Elmegreen, B.G. et al. 2015, *MNRAS*, 452, 3508
- Gouliermis, D.A., Elmegreen, B.G., Elmegreen, D.M. et al. 2017, *MNRAS*, 468, 509
- Grasha, K., Calzetti, D., Adamo, A. et al. 2017, *ApJ*, 815, 93
- Grasha, K., Calzetti, D., Adamo, A. et al. 2017, *ApJ*, 840, 113
- Grasha, K., Elmegreen, B.G., Calzetti, D., et al. 2017, *ApJ*, 842, 25
- Gregorio-Hetem, J., Hetem, A., Santos-Silva, T. & Fernandes, B. 2015, *MNRAS*, 448, 2504
- Gusev, A. S. 2002, *A&AT*, 21, 75
- Gutermuth R. A. et al., 2008, *ApJ*, 674, 336
- Harris, J., & Zaritsky, D. 1999, *AJ*, 117, 2831
- Heydari-Malayeri, M., Charmandaris, V., Deharveng, L., Rosa, M.R., Schaerer, D., & Zinnecker, H. 2001, *A&A*, 372, 495
- Ivanov, G.R. 2005, *PASRB*, 4, 75
- Johnstone, D., Wilson, C. D., Moriarty-Schieven, G., et al. 2000, *ApJ*, 545, 327
- Larson, R.B. 1995, *MNRAS*, 272, 213
- Maragoudaki, F., Kontizas, M., Kontizas, E., Dapergolas, A., & Morgan, D.H. 1998, *A&A*, 338, L29
- Miville-Deschênes, M.-A., Murray, N., Lee, E.J. 2017, *ApJ*, 834, 57
- Nanda Kumar, M.S., Kamath, U.S., & Davis, C.J. 2004, *MNRAS*, 353, 1025
- Odekon, Mary Crone 2006, *AJ*, 132, 1834
- Odekon, M.C. 2008, *ApJ*, 681, 1248
- Payne-Gaposchkin, C. H. 1974, *SCoA*, 16, 2
- Pietrzyn'ski, G., Gieren, W., Fouqué, P., & Pont, F.A. 2001, *A&A*, 371, 497
- Sánchez, N., Alfaro, E.J., Elias, F., Delgado, A.J., & Cabrera-Caño, J. 2007, *ApJ*, 667, 213

- Sánchez, N., & Alfaro, E.J. 2008, ApJS, 178, 1
- Sánchez, N. & Alfaro, E.J. 2009, ApJ, 696, 2086
- Sánchez, N. & Alfaro, E.J. 2010, in Lecture Notes and Essays in Astrophysics, vol. 4, Edited by A. Ulla and M. Manteiga (Trculo Press: Vigo, Spain). ISBN: 978-84-936098-8-7, p. 1-11
- Scheepmaker, R. A., Lamers, H. J. G. L. M., Anders, P., & Larsen, S. S. 2009, A&A, 494, 81
- Simon, M. 1997, ApJ, 482, L81
- Smith, M. D., Gredel, R., Khanzadyan, T., & Stankeinst, T. 2005, MmSAI, 76, 247
- Testi, L., Sargent, A.I., Olmi, L., & Onello, J.S., 2000, ApJ, 540, L53
- Willett, K.W., Elmegreen, B.G. & Hunter, D.A. 2005, AJ, 129, 2186
- Zhang, Q., Fall, S. M., & Whitmore, B. C. 2001, ApJ, 561, 727

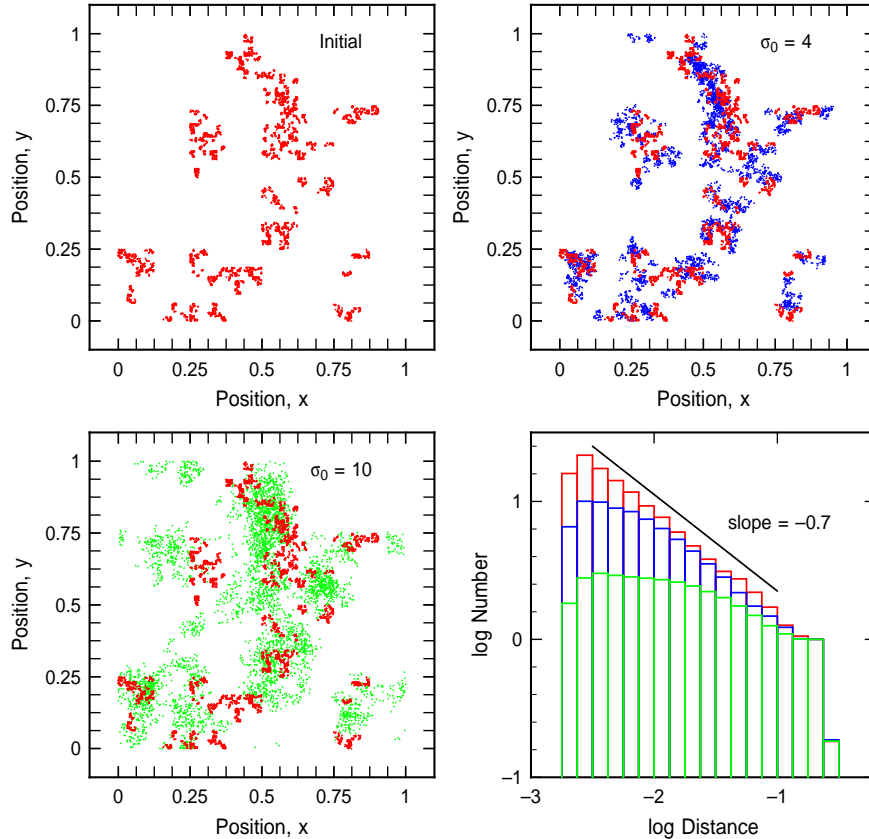


Fig. 1.— The positions of stars in a fractal model are shown. In the upper left they have their initial state, in the upper right they have been given random displacements (blue points) with amplitude $\sigma_0 = 4$ (see text), and in the lower left they have been given larger random displacements (green points) with $\sigma_0 = 10$. The initial state is repeated as red points for comparison. The histograms in the lower right are the TPCFs with colors corresponding to the points; each TPCF is an average of 10 random trials with the same parameters but different random initial conditions. The initial TPCF (red) is a power law with a slope of -0.7 as expected for the fractal dimension on a plane, $D = 1.3$. As the stars move randomly, increasing their excursions over time (from red to blue to green point distributions), the power law bends over first at small scales and then continues to bend over at larger scales.

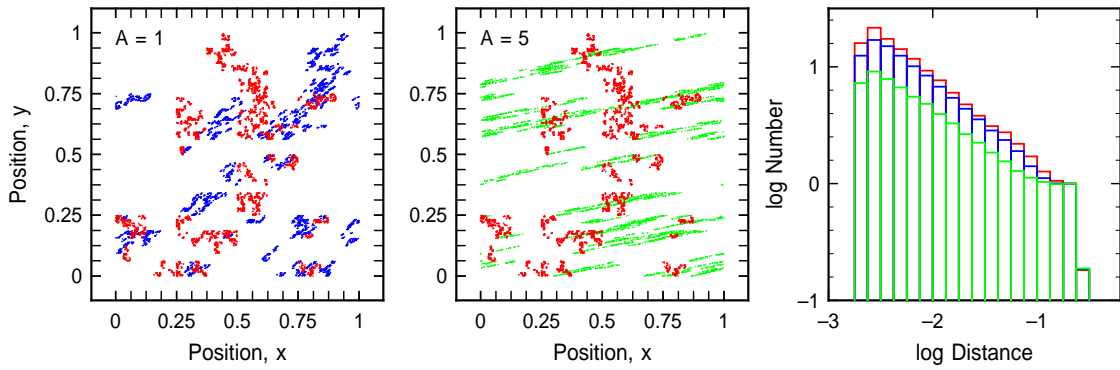


Fig. 2.— The positions of stars in the fractal model with shear increasing from red points (initial state) to blue to green, as measured by the shear variable $A = 1$ and $A = 5$ (see text). The TPCFs are shown with the same colors as the points (each is an average of 10 trials). The TPCF flattens first at large scales because shear moves stars apart most on large scales, but the overall flattening is limited by the remaining correlation in the azimuthal direction (horizontal in the figures).

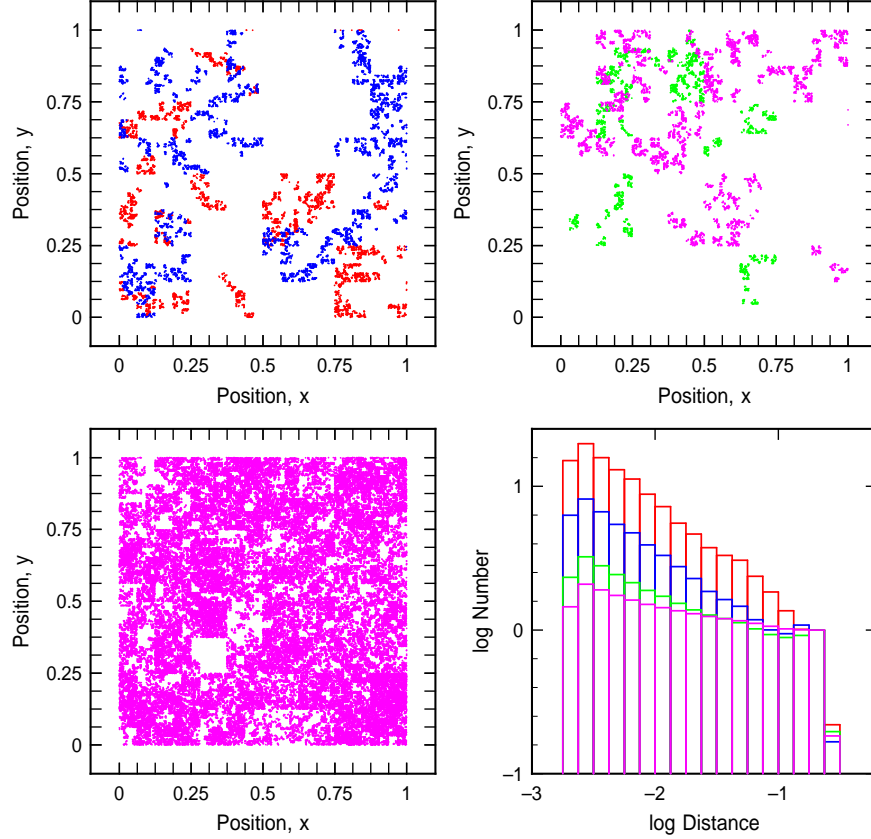


Fig. 3.— The positions of stars in a superposition of fractal models, with no random motions or shear. The top left panel shows the most recent population of stars (the 20th generation) as red points and the next most recent as blue points, both in their original positions in the absence of random motions and shear. The red histogram is the TPCF for the one case with red points, and the blue histogram is the TPCF for the sum of the red and blue points, taken as a composite spatial distribution. This blue TPCF shows a flattening at large scales because the two populations overlap most on these scales, but the power law is about the same as for a single population on small scales because each population is still directly visible on small scales. In the upper right, the magenta points are the first population out of 20 to form, and the green points are the 11th generation. These points also have their initial positions because in this figure there are no random motions nor shear. The lower left panel shows all of the 20 generations superposed. The green histogram is from the superposition of the first 11 generations to form and the magenta histogram is from the superposition of all of them.

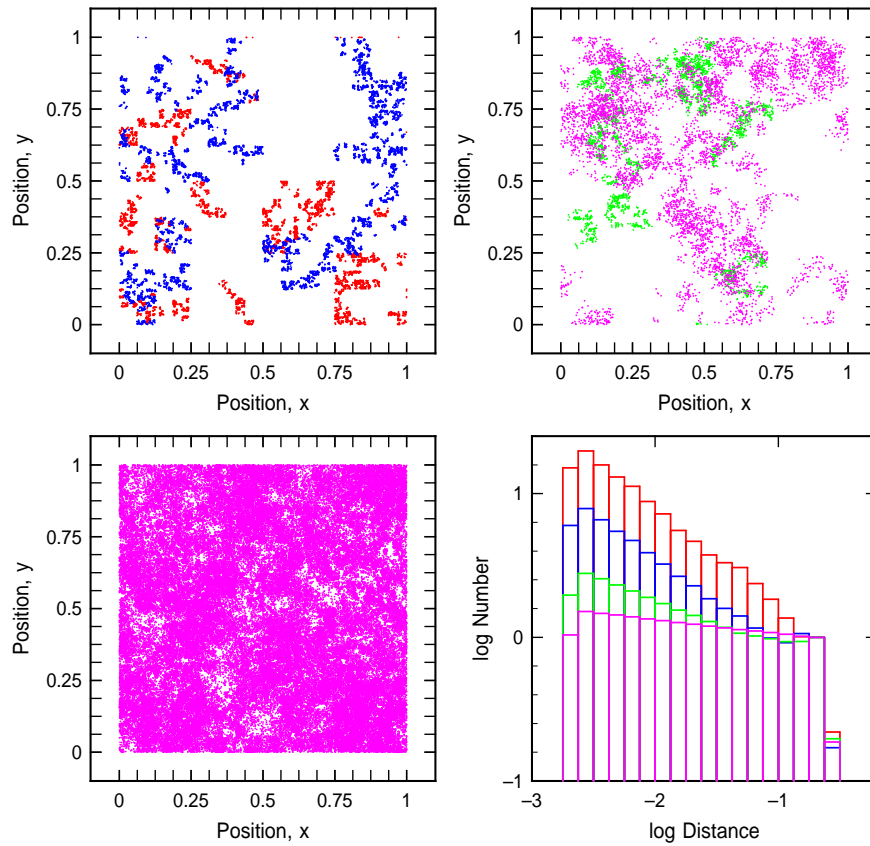


Fig. 4.— The positions of stars in a superposition of fractal models, this time with random motions but still no shear. The points have the same colors as in Figure 3 but now the effect of aging and increased dispersal are evident. The youngest population (20th generation) is red, the next youngest is blue, the 10th youngest (the 11th to form) is green and the oldest, or 1st generation, is magenta. The histograms flatten first at large scales, but random motions supplement this flattening at small scales and the result is a steady decrease in the slope of the power law.

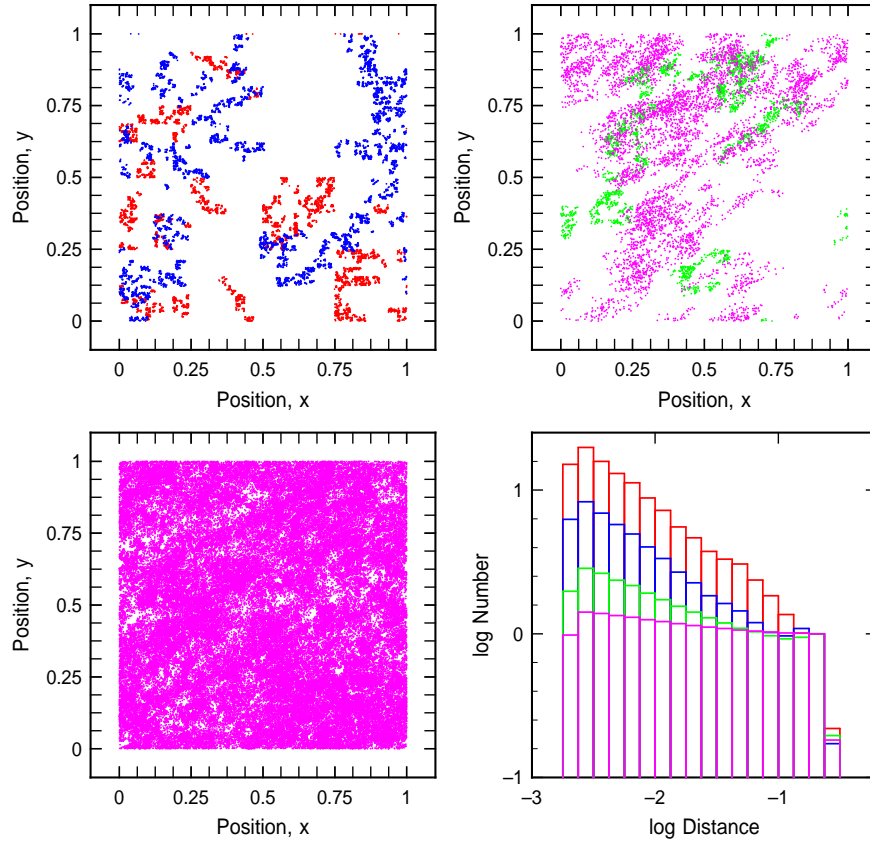


Fig. 5.— The positions of stars in a superposition of fractal models, this time with both random motions and shear. The points have the same colors as in Figures 3 and 4. Shear has relatively little additional affect on the TPCFs.